RFI Detection and Mitigation for AMSR-E Ocean Retrievals

Kyle Hilburn, Chelle Gentemann, Marty Brewer,
Lucrezia Ricciardulli, and Frank Wentz
Remote Sensing Systems
Santa Rosa, CA, USA
hilburn@remss.com

***Abstract* – Microwave observations provide physically-based retrievals for several essential climate variables over the ocean. RFI over the ocean is rapidly increasing in area, and it can produce errors of several degrees in monthly average SST if no removal or mitigation is used. We examine the spatial and temporal patterns of RFI over the ocean for the AMSR-E sensor.**

Keywords – Microwave radiometry; Radiofrequency interference; Earth Observing System; Low Earth orbit satellites; Oceans

I. Introduction

Passive microwave measurements from 6-37 GHz provide a wealth of geophysical information over the ocean. Remote Sensing Systems (RSS) uses that information to provide physically-based retrievals of sea surface temperature through clouds, surface wind speed, surface wind direction, total precipitable water vapor, total cloud liquid water, and surface rain rate.

The channel bandwidths used for Earth observation are typically much wider than the very limited protected bands allocated for microwave remote sensing. Radio frequency interference (RFI), long recognized as a problem for geophysical retrievals over land [1], is also a problem over the ocean. The primary source of ocean RFI is television broadcasts from geostationary satellites, reflected off the ocean surface and into the field of view of Earth observing sensors. The other source is direct emission from surface-based sources that produce a very strong signal over a localized area. Both forms of RFI are a rapidly growing problem, which has been addressed at RSS using detection and removal of contaminated observations. As the area of ocean covered by RFI increases, removal becomes a less attractive option and mitigation strategies should be considered.

II. Methodology

RFI is identified by calculating the difference between sea surface temperature (SST) retrievals from RSS Version-7 standard all-channel retrieval algorithm (using 6.9, 10.7, 18.7, 23.8, and 36.5 GHz) with SST retrievals from a No-10 GHz algorithm. The training procedure for the No-10 algorithm is the same as the standard algorithm, and it uses the same multi-stage linear regression approach as the standard algorithm [2]. The algorithm is physically-based; minimizing the difference between measured and modeled brightness temperatures using RSS radiative transfer model [3]. The retrievals were averaged onto monthly-mean 0.25-deg latitude-longitude maps, separated by ascending and descending passes.

There are random differences between the standard and No-10 algorithms that are not due to RFI. These differences are generally small. Inspection of the cumulative distribution function gives that, globally, 95% of the monthly-mean differences are less than 0.2 K and 99% are less than 0.3 K. To be certain that we isolate RFI, we used a threshold of 0.5 K. Fig. 1 indicates that 0.5 K marks an inflection point where the probability distribution function for ascending and descending passes separate from one another. For AMSR-E, descending orbit segments have a reflected view of the geostationary belt in the Northern Hemisphere, where most of the RFI is located. This means that differences larger than 0.5 K are very likely to be due to space-based ocean-reflected RFI. The differences in ascending passes greater than 0.5 K are primarily due to surface-based RFI.

RFI always has an additive effect on brightness temperature (TB). However, its effect on SST retrievals may be positive or negative, depending on the spectral characteristics of the RFI. Table 1 gives the standard minus No-10 SST differences for a variety of TB perturbations. TBs were perturbed about a true state given by the RSS RTM with SST of 20°C, wind speed of 7 m/s, water vapor of 30 mm, and cloud water of 0.03 mm, measured at an Earth incidence angle of 55°. When the TBs are not perturbed, the standard and No-10 algorithms give the same result to better than 0.01 K. As would be expected, perturbing 10V produces a positive bias (standard > No-10), but the difference is negative if 10H is perturbed instead. Correspondingly, if the RFI is at 6 GHz, the sign of the difference is opposite to that of 10 GHz. In this case, the standard is closer to truth than No-10. Perturbations at 18 GHz and perturbations of V and H together produce smaller SST differences.

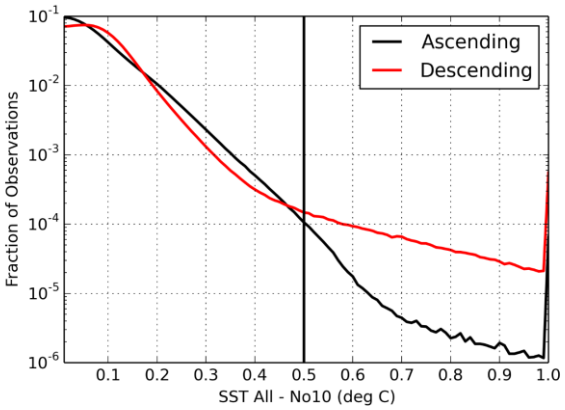

Fig. 1. Histogram of AMSR-E standard minus No-10 GHz SST differences.

TABLE 1. SST difference for a 1 K perturbation in TB.

TB Perturbation (K)	Standard – No10 SST (K)
None	-0.008
6V	-0.416
6H	0.239
10V	0.647
10H	-0.598
18V	-0.185
18H	0.133
6V and 6H	-0.192
10V and 10H	0.064
18V and 18H	0.000

III. RESULTS

RFI is highly variable in time. To characterize the RFI over the full AMSR-E period of operation, we calculated the exceedance frequency, defined as the number of times the 0.5 K threshold was exceeded, divided by the total number of valid observations in that pixel. Thus, an exceedance frequency of 0.5 means that half of the months during the 2003-2011 time period have RFI exceeding the 0.5 K level.

Inspection of global maps of exceedance frequency reveals four regions with large areas of RFI: (a) United Kingdom, (b) Mediterranean and Black Sea, (c) North America, and (d) Arabian Sea. Isolated pixels exceeding the 0.5 K threshold occur in nearly all coastal locations at one time or another, but they are not readily apparent in global maps.

Separately tracking the positive exceedance events (>0.5 K) and the negative exceedance events (<-0.5 K), we were able to separate RFI around the United Kingdom (negative) with RFI from the Mediterranean Sea (positive). It also allows separation of space-based RFI over the North Sea (negative) with surface-based RFI (positive).

Fig. 2a shows the United Kingdom region (20°W to 10°E, 45°N to 65°N). The North Sea is completely covered by RFI that is present in half or more of the months. This RFI is also present in the North Atlantic. It extends from Ireland south along the west coast of France in the Bay of Biscay. The RFI is present as far south as the Mediterranean Sea on the southern coast of France. The bright spot at 60.6°N, 2.8°E is in the vicinity of Oseberg Oil Field. Less frequent RFI is also present along the west coast of Norway, northern coast of Spain, and west coast of Portugal. There are other fragments in the Tyrrhenian Sea and Adriatic Sea, as well as in the Baltic Sea between Sweden and Poland.

For the UK region (Fig. 3a), RFI has been present for the whole period of AMSR-E. Direct-broadcast services began in Europe with the Astra 1A satellite in 1988. Transmissions are at 10.7-12.75 GHz in this region. Currently, there are at least 16 operational Astra satellites in orbital locations from 5°E to 31.5°E. Over the UK region, RFI area has increased by 19%/decade.

Fig. 2b shows the Mediterranean Sea and Black Sea region (0°E to 40°E, 30°N to 50°N). The most frequent RFI is located in the Tyrrhenian Sea, but RFI is present basin-wide and extends in to the Black Sea. The intense spot in the Dutch Sector of the North Sea at 54.0°N, 4.5°E is near several oil rigs.

RFI in the Mediterranean region (Fig. 3b) covers more than 20% of the basin starting in 2006, the same year Hot Bird 4 was redeployed as Atlantic Bird 4 / Nilesat 103. Hot Bird 7A and 8 was both launched in 2006. Hot Bird 8 is among the largest and most powerful broadcast satellites for Europe. Hot Birds 9 and 10 were launched in 2008 and 2009. RFI area has increased by 45%/decade over this region.

Fig. 2c shows the North American region (130°W to 65°W, 20°N to 50°N). RFI extends all along the U.S. west coast from Canada to Mexico, along the Gulf Coast and Florida, and all along the east coast from Florida to Canada. An oil platform is located at 27.9°N, 93.6°W where the bright spot in the Gulf of Mexico is located in Fig. 2c. Additional surface-based RFI can be seen on the northern coast of the Dominican Republic and Puerto Rico.

The North American region (Fig. 3c) was free of RFI until 2007. This changed after launch of DirectTV-10 in July 2007, followed by DirectTV-11 in 2008, and DirectTV-12 in 2009. This RFI is at 18 GHz. RFI area has increased by 9%/decade.

Fig 2d shows the Arabian Sea region. The RFI in this region is all surface-based and is at 6 GHz. The large cluster at 19.4°N, 71.6°E is collocated with the Bombay High oil rig.

RFI in the Arabian Sea region (Fig. 3d) covered 0.5% starting in 2005 and experience a large increase from 2011-2012. RFI area has increased by 2%/decade.

The spatial patterns of RFI clearly resemble space-based sources reflected from the ocean surface. We traced the reflection of the satellite boresight vector from the ocean surface up to geostationary altitude. For the regions we have identified as being space-based RFI, these vectors crossed at latitudes within ±5° of the Equator. This confirms that the sources are from geostationary satellites. When a histogram is made of the geostationary crossing longitudes, distinct peaks form at the orbit slot locations. These can be used to further identify the particular satellite from which the RFI is originating.

Identification of the strong seasonal cycles in space-based RFI are a new result. There are two geophysical factors known to influence RFI. The first is wind speed, which roughens the ocean surface and causes RFI to be spread-out over a larger area. The second is rain, which attenuates the RFI and reduces the area. Fig. 4 compares the UK and Mediterranean RFI time series with collocated WindSat observations of wind speed and rain rate for which RFI has been removed. Over the UK, there is a strong positive correlation between the wind speed and the RFI area. Over the Mediterranean, there is an inverse correlation between the RFI area and the area covered by rain. The RFI area curve has flat minima in the wintertime, unlike the rain curve. However, the flat minima corresponding to zero RFI area do not really indicate that there is no RFI. Rather, that it has fallen below the 0.5 K threshold used for this analysis.

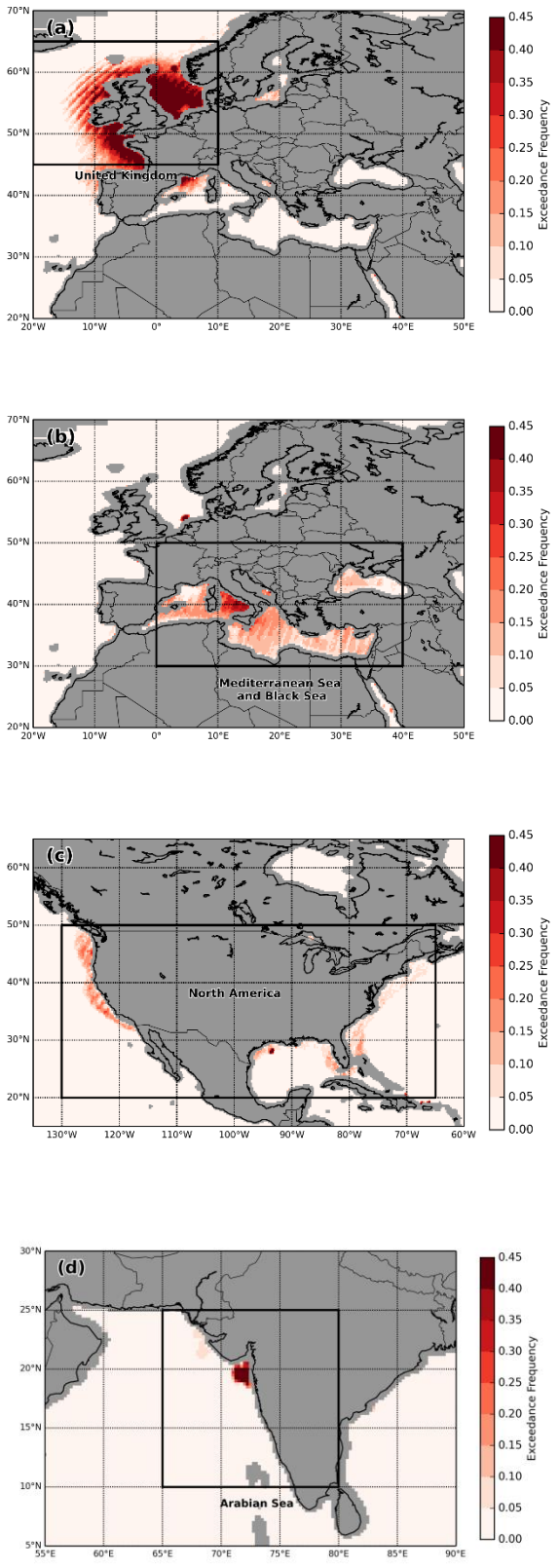

Fig. 2. Maps of SST exceedance frequency for (a) United Kingdom, (b) Mediterranean and Black Sea, and (c) North America, and (d) Arabian Sea.

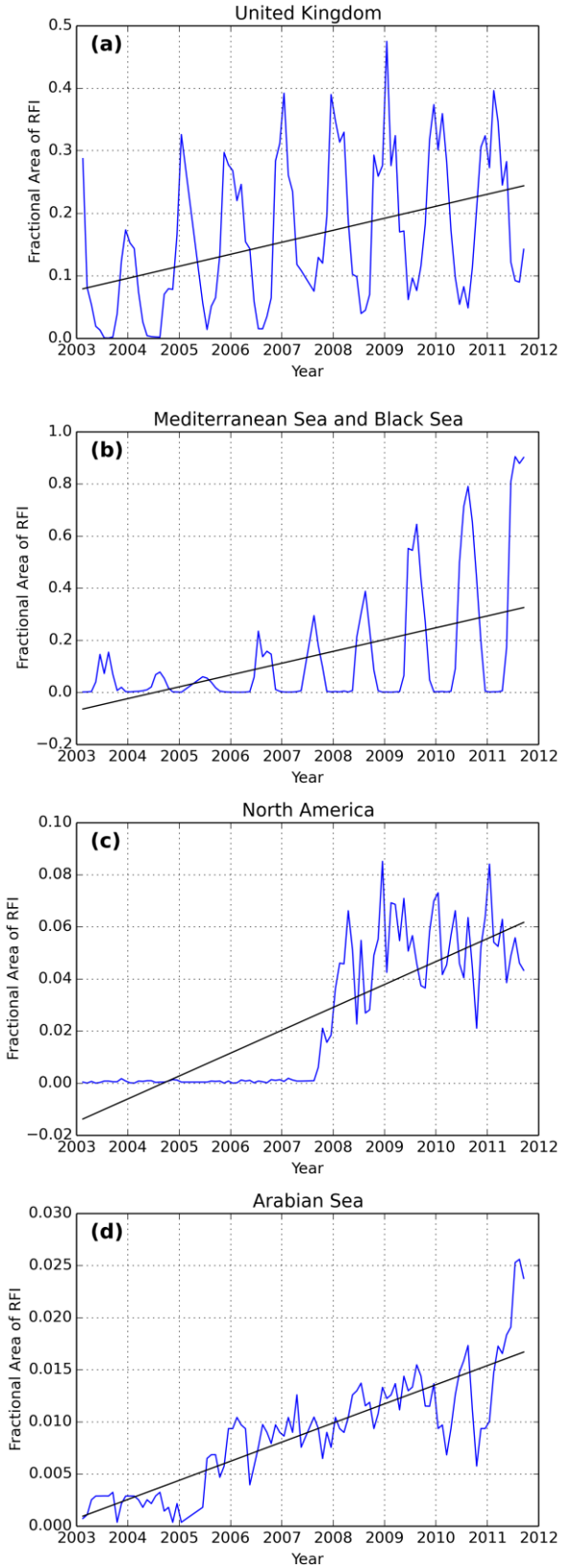

Fig. 3. Time series of RFI area for (a) United Kingdom, (b) Mediterranean and Black Sea, (c) North America, and (d) Arabian Sea.

The No-10 algorithm has skill not only in detecting RFI but also in mitigating RFI. We calculated the standard deviation between Reynolds OI SST [4] and SST retrievals from the all-channel standard algorithm and the No-10 algorithm. Anywhere around Europe, the standard algorithm (with no RFI removal) has standard deviations around 1.5 K, with values > 2 K in the most intense spots. The No-10 algorithm has standard deviations around 0.6 K relative to Reynolds in these same locations. The No-10 GHz algorithm successfully removes the UK and Mediterranean region space-based RFI, but does not remove the ground-based RFI at 6 GHz.

IV. Conclusions

An analysis of SST retrievals made using RSS all-channel algorithm compared with retrievals made using no 10 GHz channel were able to identify areas with RFI. We were able to identify both space-based ocean-reflected RFI and surface-based direct RFI. We identified 10 GHz RFI in the North Sea, North Atlantic, Mediterranean Sea, and Black Sea. Around North America, 18 GHz RFI was identified. Surface-based RFI at 6 GHz related to oil and gas exploration was found.

As a general rule of thumb, there is the potential for RFI whenever an Earth observing sensor:

1) has a reflected view of the geostationary orbital belt, or
2) observes a part of the ocean where there is active oil or gas exploration.

This analysis was limited to AMSR-E, and it would be interesting to extend the analysis to AMSR2. We have already identified new RFI in AMSR2. There are long (in latitude) narrow streaks of RFI off the west coast of Mexico that we have confirmed are due to satellite phone transmissions.

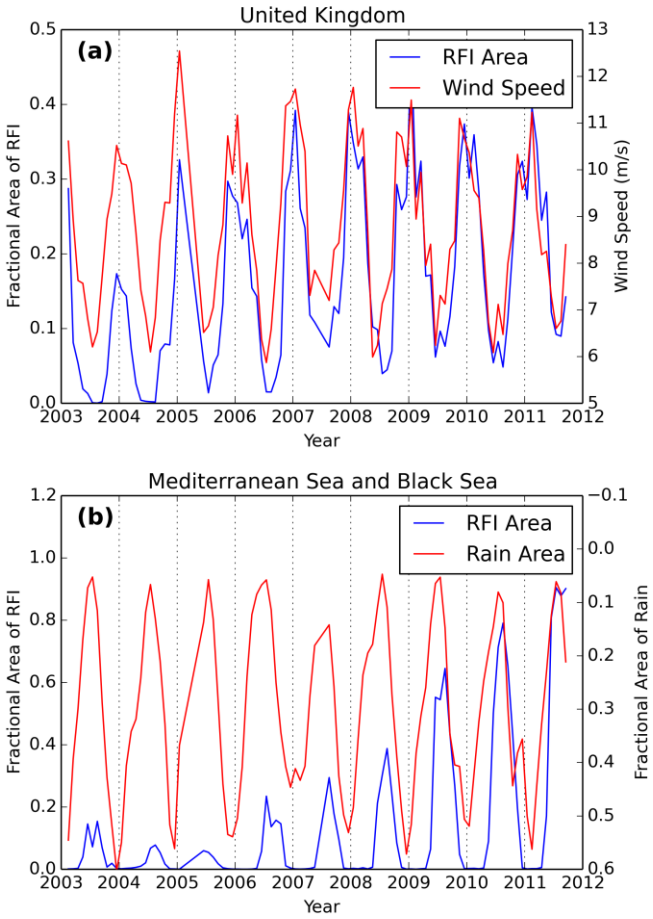

Fig. 4. Time series comparing RFI area with (a) wind speed for the UK region, and (b) rain area for the Mediterranean region. Note that on panel (b), the rain area fraction axis is reversed.

Acknowledgment

This work was supported by NASA contract NNH11CC91C "Maintaining, Refining, and Extending AMSR-E Geophysical Products and Science".

References

[1] E. G. Njoku, P. Ashcroft, T. K. Chan, and L. Li, "Global survey and statistics of radio-frequency interference in AMSR-E land observations," IEEE Trans. Geosci. Rem. Sens., vol. 43, pp. 938-947.

[2] F. J. Wentz and T. Meissner, "AMSR Ocean Algorithm," RSS Tech. Report 121599A-1, 66 pp.

[3] T. Meissner and F. J. Wentz, "The emissivity of the ocean surface between 6-90 GHz over a large range of wind speeds and Earth incidence angles," IEEE Trans. Geosci. Rem. Sens., vol. 50, pp.3004-3026.

[4] R. W. Reynolds, N. A. Rayner, T. M. Smith, D. C. Stokes, and W. Wang, "An improved in situ and satellite SST analysis for climate," J. Climate, vol. 15, pp. 1609-1625.